




# Zidovudine-Mediated Autophagy Inhibition Enhances Mitochondrial Toxicity in Muscle Cells

H. Lin,<sup>a</sup>  M. V. Stankov,<sup>a</sup> J. Hegermann,<sup>b</sup> R. Budida,<sup>a</sup> D. Panayotova-Dimitrova,<sup>c</sup> R. E. Schmidt,<sup>a</sup> G. M. N. Behrens<sup>a,d</sup>

<sup>a</sup>Department for Clinical Immunology and Rheumatology, Hannover Medical School, Hannover, Germany

<sup>b</sup>Research Core Unit for Electron Microscopy, Hannover Medical School, Hannover, Germany

<sup>c</sup>Department of Dermatology and Allergology, RWTH Aachen University Hospital, Aachen, Germany

<sup>d</sup>German Center for Infection Research (DZIF), Hannover-Braunschweig, Germany

**ABSTRACT** Nucleoside reverse transcriptase inhibitors (NRTI), such as zidovudine (AZT), are constituents of HIV-1 therapy and are used for the prevention of mother-to-child transmission. Prolonged thymidine analogue exposure has been associated with mitochondrial toxicities to heart, liver, and skeletal muscle. We hypothesized that the thymidine analogue AZT might interfere with autophagy in myocytes, a lysosomal degradation pathway implicated in the regulation of mitochondrial recycling, cell survival, and the pathogenesis of myodegenerative diseases. The impact of AZT and lamivudine (3TC) on C2C12 myocyte autophagy was studied using various methods based on LC3-green fluorescent protein overexpression or LC3 staining in combination with Western blotting, flow cytometry, and confocal and electron microscopy. Lysosomal and mitochondrial functions were studied using appropriate staining for lysosomal mass, acidity, cathepsin activity, as well as mitochondrial mass and membrane potential in combination with flow cytometry and confocal microscopy. AZT, but not 3TC, exerted a significant dose- and time-dependent inhibitory effect on late stages of autophagosome maturation, which was reversible upon mTOR inhibition. Inhibition of late autophagy at therapeutic drug concentrations led to dysfunctional mitochondrial accumulation with membrane hyperpolarization and increased reactive oxygen species (ROS) generation and, ultimately, compromised cell viability. These AZT effects could be readily replicated by pharmacological and genetic inhibition of myocyte autophagy and, most importantly, could be rescued by pharmacological stimulation of autophagolysosomal biogenesis. Our data suggest that the thymidine analogue AZT inhibits autophagy in myocytes, which in turn leads to the accumulation of dysfunctional mitochondria with increased ROS generation and compromised cell viability. This novel mechanism could contribute to our understanding of the long-term side effects of antiviral agents.

**KEYWORDS** autophagy, myocyte, heart, skeletal muscle, HIV infection, antiretroviral therapy

Nucleoside reverse transcriptase inhibitors (NRTIs), such as zidovudine (AZT), are part of numerous regimens for the treatment of HIV infection or for the prevention of mother-to-child transmission (MTCT), particularly in resource-poor HIV/AIDS populations (1). Prolonged NRTI exposure to thymidine analogues has been associated with mitochondrial toxicities to heart, liver, and skeletal muscle (2, 3). NRTI-mediated mitochondrial toxicity accompanied by mitochondrial DNA (mtDNA) depletion has been suggested to be the central pathogenic mechanism, and some risk factors for the development of lactic acidosis, such as female gender, pregnancy, and increased body mass index, have been recognized (4–8). Biopsy specimens from patients receiving long-term treatment with AZT revealed clinical evidence of compromised mitochon-

**Citation** Lin H, Stankov MV, Hegermann J, Budida R, Panayotova-Dimitrova D, Schmidt RE, Behrens GMN. 2019. Zidovudine-mediated autophagy inhibition enhances mitochondrial toxicity in muscle cells. *Antimicrob Agents Chemother* 63:e01443-18. <https://doi.org/10.1128/AAC.01443-18>.

**Copyright** © 2018 American Society for Microbiology. All Rights Reserved.

Address correspondence to G. M. N. Behrens, behrens.georg@mh-hannover.de.

H.L. and M.V.S. contributed equally to this article.

**Received** 10 July 2018

**Returned for modification** 31 July 2018

**Accepted** 15 October 2018

**Accepted manuscript posted online** 29 October 2018

**Published** 21 December 2018

drial function that deteriorates over the duration of NRTI treatment (9). It has been demonstrated that NRTI-induced mitochondrial toxicity increases reactive oxygen species (ROS) production and amplifies mitochondrial dysfunction and that antioxidants counteract the NRTI-induced toxicity both *in vitro* and *in vivo* (10–12). Thus, it is conceivable to expect that the potential cumulative side effects of NRTIs may lead to long-term tissue damage in the population aging with HIV/AIDS (13–15). In that regard, long-term therapy with zidovudine has been associated with a toxic mitochondrial myopathy (16) and myocyte mitochondrial dysfunction with increased ROS production, confirmed by both *in vitro* and *in vivo* studies (2, 3, 10, 11, 17, 18).

Interestingly, most of the events related to zidovudine exposure, such as accumulation of dysfunctional mitochondria, increased ROS production, and compromised cell viability, have also been associated with autophagy inhibition *per se* (19–21), and compromised autophagolysosomal activity has been implicated in the pathogenesis of myodegenerative diseases (22). For example, Danon disease, a genetic disease characterized by cardiomyopathy and myopathy, is related to a mutation in the lysosomal protein lysosome-associated membrane protein 2 (LAMP-2) and is associated with the profound accumulation of autophagosomes in the muscles of LAMP-2-deficient mice and patients potentially due to reduced autophagolysosomal fusion (23). Murine models with heart-specific autophagy deficiency due to *ATG5* knockout reveal cardiac hypertrophy and contractile dysfunction in association with mitochondrial structural abnormalities (24).

Despite considerable progress in our understanding of how thymidine analogues might damage mitochondria (25, 26), little is still known about their effect on the elimination and recycling of dysfunctional mitochondria in myocytes. Autophagolysosomal removal of dysfunctional mitochondria, however, relates to the depletion of proapoptotic signals and, thus, serves as an integral part of the maintenance of cellular homeostasis and survival (27).

We hypothesized that along with the well-characterized mitochondrial toxicity of thymidine analogues, these drugs have the ability to compromise myocyte autophagy. We expected that this would cause impaired clearance of dysfunctional mitochondria, increased ROS production, and, ultimately, compromised cell viability. We therefore speculated that these effects could help to explain the development of long-term side effects in cardiomyocytes or skeletal muscle cells in HIV/AIDS patients receiving anti-retroviral treatment.

## RESULTS

**AZT induces autophagosome accumulation.** Using cells stably expressing LC3-green fluorescent protein (GFP) and fluorescence microscopy analysis, autophagosomes are detected as punctae formation on the background of a homogeneously distributed LC3-GFP pattern. Under these conditions, induction of autophagy is identified as the accumulation of autophagic punctae. Early autophagy inhibition can be recognized by the inability of the cell to form autophagic punctae under conditions leading to autophagy activation. On the other hand, inhibition of late autophagy is estimated to produce additional autophagosome accumulation. In order to evaluate the effects of NRTIs on myocyte autophagic activity, we cultured C2C12 cells stably expressing LC3-GFP with and without high concentrations of AZT (257  $\mu$ M) or lamivudine (3TC; 262  $\mu$ M) for 48 h or with 3-methyladenine (3MA; 10 mM) or nocodazole-vinblastine (25  $\mu$ M) for 5 h. A parallel set of cells under the above-mentioned conditions was supplemented with a small-molecule mTOR inhibitor and autophagy activator PP242 (5  $\mu$ M) for the last 4 h (Fig. 1A). PP242 is a dual mTORC1 and mTORC2 inhibitor which targets the catalytic domain of mTOR in an ATP-competitive manner (28). Our preliminary testing revealed that PP242 successfully inhibits mTOR phosphorylation, leading to the decreased phosphorylation of downstream targets, such as eukaryotic initiation factor 4E-binding protein 1 (4E-BP1), and increased autophagy degradation of autophagy substrates, such as P62 (data not shown). Fluorescence microscopy examination of control cultures revealed a homogeneously distributed LC3-GFP pattern

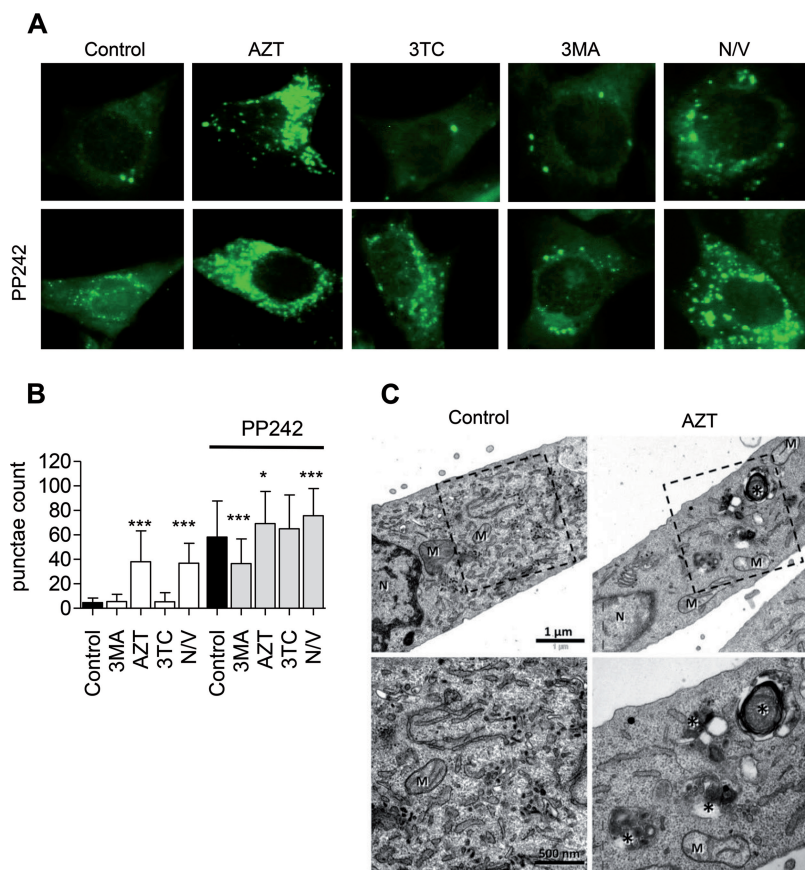


**FIG 1** Zidovudine (AZT) causes an increase in autophagosomes in C2C12 cells. (A) Fluorescence microscopy of C2C12 cells stably expressing LC3-GFP treated for 48 h with AZT (257  $\mu$ M) or 3TC (262  $\mu$ M) or for 5 h with 3MA (10 mM) or nocodazole-vinblastine (N/V; 25  $\mu$ M), in the presence or absence of PP242 (5  $\mu$ M) for the last 4 h. Pictures are representative of those from at least three independent experiments. (B) Average number of punctae per cell under each of the 10 conditions. Fifty cells were randomly counted per condition per experiment in three independent experiments. Conditions without PP242 were analyzed in comparison to the control conditions, while conditions with PP242 were analyzed in comparison to conditions with PP242 alone. (C) Transmission electron microscopy images of C2C12 cells treated with AZT for 72 h. Note the accumulation of autophagy-related compartments (indicated by asterisks) in the AZT-treated sample. M, mitochondria; N, nucleus. (Top) Overview; (bottom) higher magnification of the boxed areas in the panels in the top row. (B) The results are presented as the distribution of the mean and are representative of those for at least 30 images from each treated condition. \*,  $P < 0.05$ ; \*\*\*,  $P < 0.001$ .

(Fig. 1A). AZT incubation resulted in a considerable increase in C2C12 autophagic punctae (Fig. 1A and B). An analogous effect was discerned with the cocktail of the fusion inhibitors nocodazole and vinblastine. As expected, the autophagy activator PP242 intensified autophagic punctae formation in control cultures. This effect was abrogated in the presence of the class III phosphatidylinositol 3 (PI3) kinase inhibitor 3-methyladenine (3MA), which inhibits the early stages of autophagosome formation (28), and was a bit stronger in coincubations with the inhibitors of autophagosome maturation nocodazole-vinblastine or AZT (Fig. 1A and B). These effects were AZT specific and were not detected using 3TC.

As autophagosomes are intermediate structures involved in a dynamic degradation process, their total cellular abundance is a function of equilibrium between newly generated autophagosomes and autolysosome degradation (28). Therefore, we expected that an AZT-mediated increase in autophagosomes is consistent with either drug-related autophagy induction or inhibition of autophagosome maturation. A qualitative comparison by electron microscopy (EM) revealed that among the profiles of the AZT-treated cells, the accumulation of autophagic compartments was easy to find, while in the control, such situations were rare (Fig. 1C).

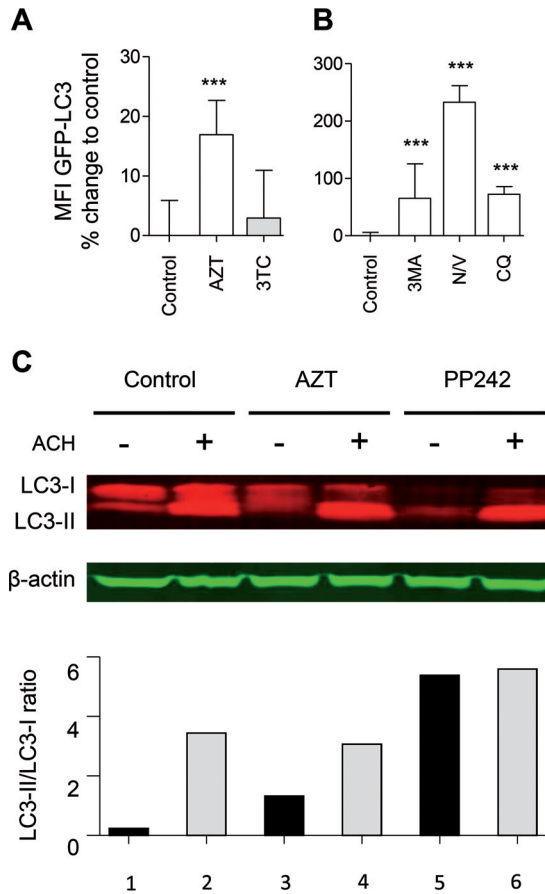


**FIG 2** AZT inhibits autophagic flux. (A) C2C12 cells stably expressing LC3-GFP were treated with AZT (8.6  $\mu$ M), 3TC (8.7  $\mu$ M), 3MA (0.2 mM), nocodazole-vinblastine (N/V; 2  $\mu$ M), or CQ (50  $\mu$ M) for 24 h. (A and B) Flow cytometry analysis of autophagic flux in C2C12 cells expressing the LC3-GFP fusion protein. Data are presented as the percent change from the value for the untreated control. C2C12 cells were treated with AZT (42.8  $\mu$ M) for 72 h or PP242 (5  $\mu$ M) for 4 h in the presence or absence of 5  $\mu$ M ACH for the last 3 h. The data in panels A and B are presented as the mean  $\pm$  SD and are representative of those from at least three independent experiments with three replicates. \*\*\*,  $P < 0.001$ . MFI, mean fluorescent intensity. (C) Western blot analyses of the conversion of LC3-I to LC3-II with and without ammonium chloride (ACH) blockage of autolysosomal degradation using whole-cell lysate and anti-LC3 and  $\beta$ -actin antibodies (top) with densitometry analysis (bottom). A representative blot from three experiments is shown.

**AZT but not 3TC inhibits autophagic flux in myocytes.** In order to measure autophagic flux, we took advantage of a highly sensitive method which is based on flow cytometric monitoring of LC3 turnover (29–32). This assay measures the autophagic process, in which LC3-II from the inner autophagosome membrane undergoes autolysosomal degradation, resulting in a gradual decrease in total cellular LC3 abundance. Therefore, in cellular models with the constitutive expression of the LC3-GFP fusion protein, an increase or decrease in autophagic flux is detected as a corresponding reduction or accumulation of the total cellular GFP signal (29–32). In order to examine the effect of NRTIs on myocyte autophagy and better distinguish between inhibition of autophagosome maturation and autophagy induction, we cultured C2C12 LC3-GFP-expressing cells with and without therapeutic maximum concentrations ( $C_{max}$ s) of AZT (8.6  $\mu$ M) or 3TC (8.7  $\mu$ M) for 24 h. In addition, the cells were incubated with 3MA (0.2 mM), nocodazole-vinblastine (20  $\mu$ M), or chloroquine (CQ; 50  $\mu$ M) (Fig. 2A and B). AZT cultures revealed substantially decreased autophagic flux, as demonstrated by the accumulation of the total cellular LC3-GFP signal (Fig. 2A). A similar decrease in autophagic flux was reproduced in all cultures containing established inhibitors of autophagy (Fig. 2B). In contrast, autophagic flux was unaffected by 3TC

incubation. Importantly, the AZT effect on autophagy was detectable at therapeutic  $C_{max}$ s (Fig. 2A).

Densitometry of semiquantitative Western blots demonstrated an AZT-mediated increase in the conversion of LC3-I to LC3-II (Fig. 2C; LC3-II/LC3-I ratio for column 3 versus column 1), which could be attributed to either enhanced autophagosome generation or inhibition of autophagosome maturation (28). In order to distinguish between these two scenarios, we evaluated autophagic flux, as determined by accumulation of the LC3-II band upon blockage of autolysosomal degradation using ammonium chloride (ACH). Blockage of autolysosomal degradation led to a substantial increase in the LC3-II/LC3-I ratio for the control (Fig. 2C; column 2 versus column 1) but to a much smaller accumulation in AZT-treated cells (Fig. 2C; column 4 versus column 3). These results are consistent with an AZT-associated activation of early stages of autophagosome formation (Fig. 2C; the LC3-II/LC3-I ratio for column 3 is bigger than that for column 1) and inhibition of late stages of autophagosome maturation and degradation (Fig. 2C; the LC3-II/LC3-I ratio for column 4 does not surpass that for column 2).

**AZT induces accumulation of dysfunctional mitochondria and ROS production in myocytes.** The generation of dysfunctional mitochondria and augmented ROS production have been documented as a result of defective autophagy (21). Therefore, we analyzed the effect of defective autophagy on total cellular mitochondrial abundance (MitoTracker Red [MTR Red] staining) and ROS production [5-(and-6)-chloromethyl-2',7'-dichlorodihydrofluorescein diacetate, acetyl ester (CM-H2DCFDA)] in C2C12 cells incubated in the presence or absence of different concentrations of AZT (6, 30, 180  $\mu$ M) or 3TC (8, 40, 240  $\mu$ M) for up to 8 days or with 3MA (5 mM) or nocodazole-vinblastine (50  $\mu$ M) for 24 h. The incubation period of 8 days was chosen as it is the minimum time period reported to be necessary for mitochondrial turnover under physiological conditions (33). Consistent with autophagy inhibition, incubation with AZT produced profound myocyte mitochondrial accumulation (Fig. 3A). In contrast, and consistent with its lack of an effect on autophagy, 3TC did not increase the mitochondrial abundance even at the highest concentration used (Fig. 3A). AZT treatment was associated with mitochondrial membrane hyperpolarization, as revealed by an AZT-mediated increase in the ratio of potential-dependent MitoTracker Deep Red (MTR Deep Red) and potential-independent MitoTracker Green (MTR Green) staining (34) (see Fig. S1A and B in the supplemental material) as well as by increased mitochondrial potential-specific MitoProbe TMRM staining (Fig. S1C and D). At the same time, AZT had no major effect on the enzymatic activity of mitochondrial respiratory chain complexes (complexes I to V) (Fig. S2), consistent with previous reports by us (35, 36). Notably, the AZT-mediated accumulation of hyperpolarized mitochondria was accompanied by increased ROS generation (Fig. 3B). Again, 3TC had no stimulatory effect on mitochondrial accumulation or ROS generation (Fig. 3B); if anything, 3TC even led to a slight decrease in both mitochondrial abundance and ROS generation. These data were consistent with the notion that basic autophagy activity is essential for the removal of damaged mitochondria and maintenance of normal mitochondrial homeostasis. Incubation with established early (3MA) and late (nocodazole-vinblastine) autophagy inhibitors reiterated the effect of AZT on both the accumulation of dysfunctional mitochondria and ROS production (Fig. S3).

Collectively, these data suggest that AZT-mediated autophagy inhibition prevents the removal of dysfunctional mitochondria produced in relation to its mitochondrial toxicity. Transmission electron microscopy examination did not demonstrate any morphological alteration in mitochondria at that time point (Fig. 3C).

**Genetic inhibition of autophagy reiterates the effects of AZT on myocytes.** Since our experiments suggested that thymidine analogue-mediated autophagy inhibition is a component of drug toxicity, we aimed to explore whether autophagy inhibition *per se* could interfere with myocyte function in our experimental model. To this end, we aimed to validate the above-mentioned observations using autophagy-specific small interfering RNA (siRNA)-mediated knockdown of ATG7 (28). Genetic



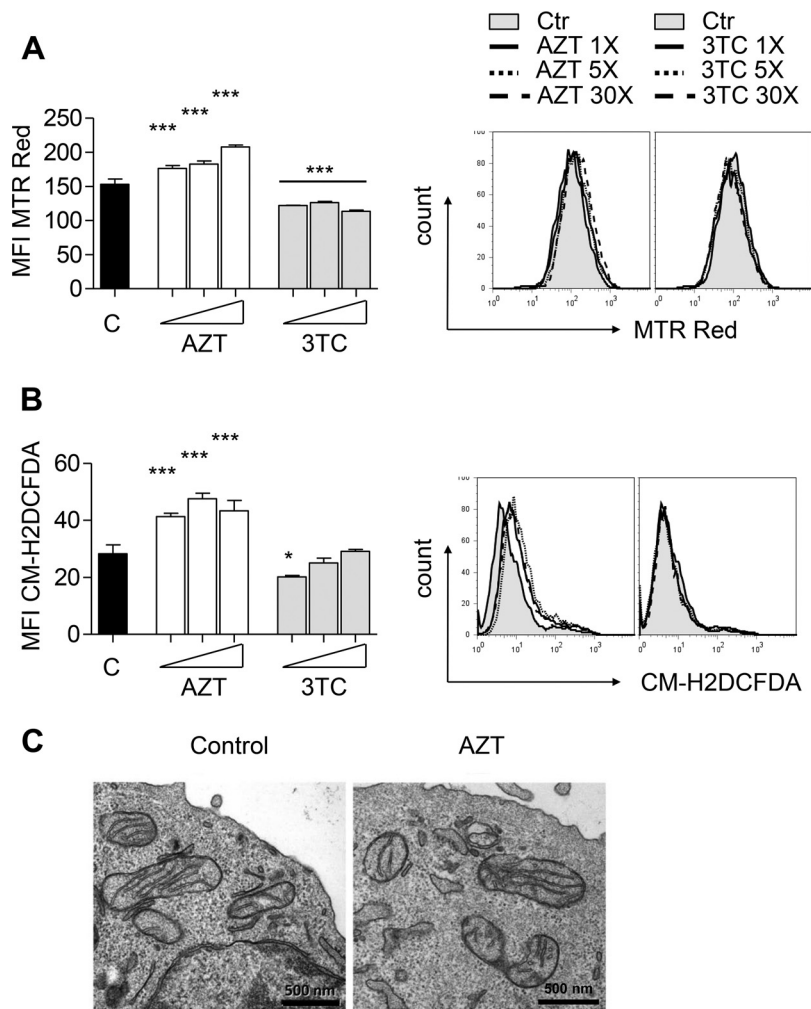


**FIG 3** AZT induces accumulation of dysfunctional mitochondria and increased ROS production. C2C12 cells were incubated in the absence or presence of AZT (6, 30, 150  $\mu\text{M}$ ) or 3TC (8, 40, 200  $\mu\text{M}$ ) for up to 8 days. (A) Flow cytometry analysis of total mitochondrial mass using MitoTracker Red (MTR Red) (left) with representative histograms (right). (B) Flow cytometry analysis of ROS generation using CM-H<sub>2</sub>DCFDA (left) with representative histograms (right). (C) Transmission electron microscopy images of C2C12 cells treated with AZT for 72 h. (A and B) The results of the experiments are presented as the mean  $\pm$  SD and are representative of those from at least three independent experiments with four replicates. \*,  $P < 0.05$ ; \*\*\*,  $P < 0.001$ . Ctr and C, control.

autophagy inhibition resulted in a substantial decrease in autophagic flux (Fig. 4A) and confirmed mitochondrial mass accumulation (Fig. 4B) with increased ROS production (Fig. 4C) in C2C12 cells. The successful reduction in ATG7 protein abundance as a result of siRNA-mediated ATG7 interference was confirmed by Western blotting (Fig. 4D). Taken together, these results suggest that both a semispecific pharmacological inhibition and a highly specific genetic inhibition of the autophagic process in myocytes are associated with the accumulation of dysfunctional mitochondria and ROS formation.

**AZT selectively hyperactivates myocyte lysosomal compartments.** The autophagic process begins with autophagosome formation and substrate capture and, upon successful autophagolysosomal fusion, culminates in substrate degradation. The whole degradation pathway has a common mode of regulation and appears to be highly synchronized (37–40). We were interested to investigate the extent to which AZT can affect autophagosomal maturation, which can subsequently affect downstream lysosomal homeostasis. We cultured C2C12 cells in the presence or absence of different concentrations of AZT (6, 30, 180  $\mu\text{M}$ ) or 3TC (8, 40, 240  $\mu\text{M}$ ) for up to 8 days. Flow

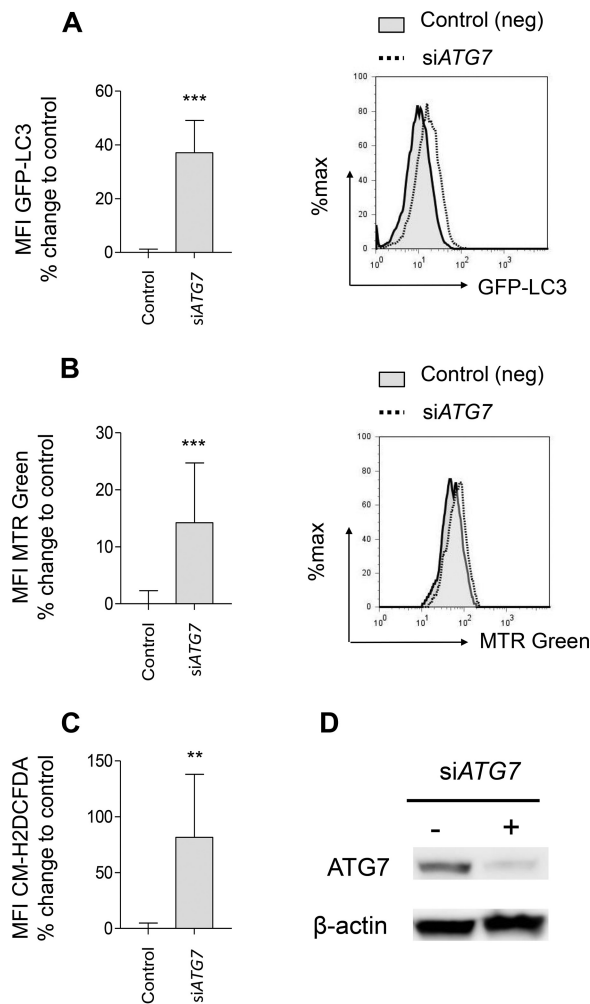


**FIG 4** Atg7 knockdown reiterates the effects of AZT on autophagy and dysfunctional mitochondrial accumulation. (A) Flow cytometry analysis of autophagic flux in C2C12 cells expressing the LC3-GFP fusion protein and treated for 72 h with control siRNA or *ATG7*-specific siRNA (si*ATG7*) (left) with representative histograms (right). Data are presented as the percent change from the value for control siRNA-treated cells. (B) Flow cytometry analysis of total mitochondrial mass using MitoTracker Red (MTR Red) in C2C12 cells treated for 72 h with control siRNA or *ATG7*-specific siRNA (left) with representative histograms (right). Data are presented as the percent change from the value for the control siRNA-treated cells. (C) Flow cytometry analysis of ROS production using CM-H2DCFDA in C2C12 cells treated for 72 h with control siRNA or *ATG7*-specific siRNA. Data are presented as the percent change from the value for the control siRNA-treated cells. (D) Western blotting evaluation of *ATG7* knockdown C2C12 cells treated with siRNA for 72 h. The results of all experiments are presented as the mean  $\pm$  SD and are representative of those from at least three independent experiments with four replicates. \*\*,  $P < 0.01$ ; \*\*\*,  $P < 0.001$ .

cytometry analyses using LysoTracker (LTR), LysoSensor (LSG), and Magic Red cathepsin B and L assays for substrate conversion demonstrated an association between the ability of AZT to compromise autophagolysosomal homeostasis and a substantial dose-dependent increase in total lysosomal abundance (Fig. 5A), acidity (Fig. 5B), as well as cathepsin B and L activity (Fig. 5C and D). Importantly, these alterations were already observed at therapeutic  $C_{max}$ s and were not detectable in the cultures with 3TC.

**AZT compromises myocyte viability.** Autophagic removal of dysfunctional mitochondria relates to the depletion of proapoptotic signals and represents an integral part of the maintenance of cellular survival and homeostasis (27). Hyperactivated lysosomal compartments in combination with dysfunctional mitochondrial accumulation and the lack of prosurvival autophagy can be expected to affect myocyte viability (41). As expected, AZT incubation for up to 8 days resulted in a dose-dependent decrease in C2C12 viability (Fig. 6). If the effect of AZT on myocyte viability is mediated

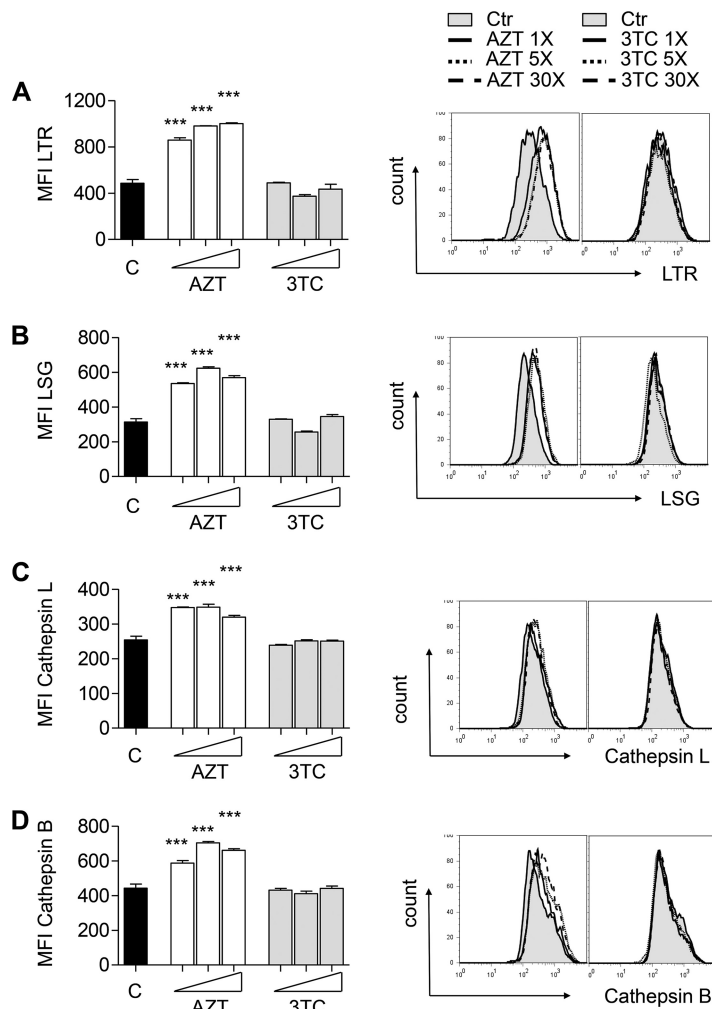


**FIG 5** AZT incubation leads to lysosomal hyperactivation. C2C12 cells were incubated in the absence or presence of AZT (6, 30, 150  $\mu$ M) or 3TC (8, 40, 200  $\mu$ M) for up to 8 days. (A) Flow cytometry analysis of total lysosomal abundance using LysoTracker Red (LTR) (left) with representative histograms (right). (B) Flow cytometry analysis of lysosomal acidity using LysoSensor Green (LSG) (left) with representative histograms (right). (C and D) Flow cytometry analysis of cathepsin L (D) and B (C) enzymatic activity using Magic Red cathepsin L and B assay kits (left) with representative histograms (right). The results of all experiments are presented as the mean  $\pm$  SD and are representative of those from at least three independent experiments with four replicates. \*\*\*,  $P < 0.001$ .

by its ability to impair autophagic removal of dysfunctional mitochondria, we would expect autophagy activation to counteract these effects, to reduce the amount of dysfunctional mitochondria, and to rescue AZT-mediated toxicity. Indeed, both long-term (8 days) and short-term (24 h) exposure to the mTOR inhibitor PP242 improved myocyte autophagic flux (Fig. 6A and B) and relieved the accumulation of dysfunctional mitochondria (Fig. 6C and D). Improved autophagic flux and a reduced abundance of dysfunctional mitochondria throughout the incubation period of 8 days rescued AZT toxicity and improved myocyte survival (Fig. 6E).

## DISCUSSION

Unfortunately, long-term NRTI exposure and, in particular, exposure to thymidine analogues have been associated with mitochondrial toxicities to heart, liver, and skeletal muscle (2, 3). AZT treatment has been associated with pathophysiological changes in cardiac mass and structure (42–44). Mechanistically, such pathophysiological changes and cardiomyopathy development have been attributed to AZT-mediated mitochondrial toxicity, characterized by mitochondrial dysfunction, mtDNA depletion,



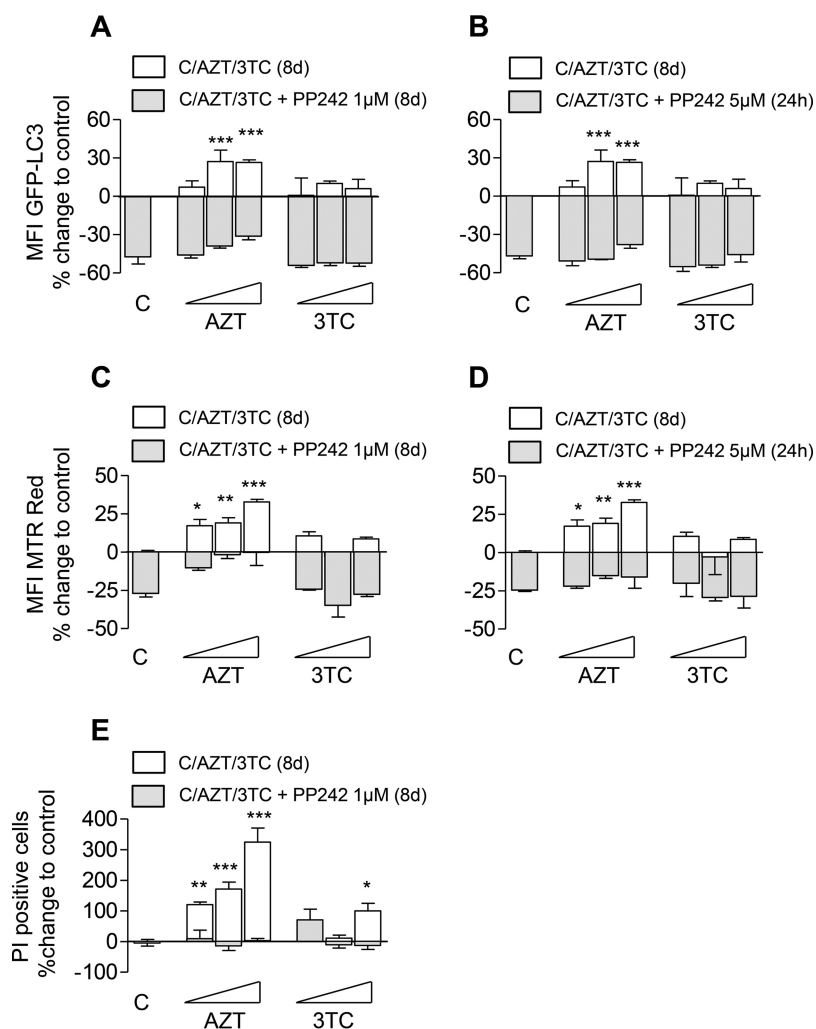


**FIG 6** Autophagy activation through mTOR inhibition improves C2C12 autophagic flux, reduces dysfunctional mitochondrial accumulation, and rescues AZT-mediated myocyte toxicity. C2C12 cells were incubated in the absence or presence of AZT (6, 30, 150  $\mu$ M) or 3TC (8, 40, 200  $\mu$ M) for up to 8 days (8d) with or without the addition of PP242. PP242 was added either for the whole incubation period of 8 days at a concentration of 1  $\mu$ M or only for the last day at 5  $\mu$ M. (A and B) Flow cytometry analysis of autophagic flux in C2C12 cells expressing the LC3-GFP fusion protein. Data are presented as the percent change from the value for the untreated control (designated C). (C and D) Flow cytometry analysis of total mitochondrial mass using MitoTracker Red (MTR Red). Data are presented as the percent change from the value for the untreated control. (E) Flow cytometry analysis of cell death using the PI exclusion assay. Data are presented as the percent change from the value for the untreated or PP242-treated control. The results of all experiments are presented as the mean  $\pm$  SD and are representative of those from at least three independent experiments with four replicates. \*,  $P < 0.05$ ; \*\*,  $P < 0.01$ ; \*\*\*,  $P < 0.001$ .

compromised energy production, and increased oxidative stress (10, 45, 46). However, despite substantial scientific progress in our understanding of how NRTIs and particularly thymidine analogues might damage mitochondria (25, 26), little attention has been given to the elimination and recycling of dysfunctional mitochondria, which is a part of the natural mechanism to maintain cellular homeostasis (27).

In the present study, we have demonstrated for the first time that AZT has the ability to inhibit late stages of myocyte autophagy. The combination of autophagosome accumulation with inhibited autophagic flux suggested that AZT stimulates early autophagosome formation but compromises late stages of autophagosome maturation and degradation. We found a robust association between the AZT-mediated suppression of autophagy and the accumulation of dysfunctional mitochondria with membrane hyperpolarization and increased ROS generation. These results provide a novel

mechanism by which AZT is able to compromise a key cellular mechanism for the recycling and elimination of dysfunctional mitochondria. Furthermore, the ability of AZT to block the late stages of the autophagic process was found to correlate with lysosomal hyperactivation and compromised myocyte viability.

The degradation pathway of autophagy is a critical intracellular process for mitochondrial turnover which targets dysfunctional mitochondria for recycling (47), and autophagy inhibition *per se* has been related to the accumulation of dysfunctional mitochondria (19–21). Our study demonstrated a close relationship between the AZT-mediated suppression of late autophagy and dysfunctional mitochondrial accumulation and an increase in ROS generation. The failure to eliminate damaged mitochondria might explain their accumulation and the ensuing decrease in myocyte viability. The participation of compromised autophagy in AZT-mediated myotoxicity in our experimental system and its clinical relevance are strongly supported by the following observations: (i) assays with independent experimental readout systems, such as confocal and electron microscopy, Western blotting, and flow cytometry, combined with assays with pharmacological inhibitors and inducers of autophagy, have led to consistent results; (ii) the results were obtained at therapeutic drug concentrations, and no effect on autophagic activity could be detected in our systems using 3TC as a control, consistent with the clinical observation of no major myotoxicity of this drug in HIV-infected patients; (iii) the effects of AZT were readily reiterated using pharmacological as well as genetic inhibitors of autophagy; and (iv) probably most importantly, pharmacological activation of myocyte autophagy reversed the AZT-mediated autophagy inhibition, alleviated the accumulation of dysfunctional mitochondria, and rescued cellular viability. The consequences of mTOR inhibition on autophagy include both the release of the mTOR-mediated block on autophagy initiation and transcription factor EB (TFEB)-mediated activation of the transcriptional program of overall autophagolysosomal biogenesis. The latter effect might explain why and how mTOR inhibition counteracts the AZT-mediated blockage in late autophagy (37–40). AZT did not inhibit early autophagosome generation but, on the contrary, increased autophagosome formation, as demonstrated by increased autophagic punctae formation, and stimulated the conversion of LC3-I to LC3-II. However, several independent assays confirmed that AZT inhibited autophagic flux, suggesting that this drug interferes with downstream events, such as autophagosome maturation. These data are consistent with clinical observations strongly associating compromised autophagolysosomal fusion with the pathogenesis of myodegenerative diseases (22).

Accumulating evidence suggests that the pathogenesis of myodegenerative diseases may involve an insufficient capacity for autophagic clearance potentially due to the failure of autophagosomes to fuse with lysosomes (22, 48). Danon disease, a genetic disease characterized by cardiomyopathy and myopathy resulting from a mutation in lysosome-associated membrane protein 2 (LAMP-2), presents as the extensive accumulation of autophagosomes in the muscles of LAMP-2-deficient mice and patients (23, 49). The link between compromised autophagosome maturation and myopathy is further supported by scientific evidence that pharmacological inhibition of the autophagosome-lysosome fusion step results in pronounced vacuolar myopathies in both rats and humans (50). Furthermore, dysregulated autophagosome-lysosome fusion has been suspected in the etiology of the pathogenesis of other muscle diseases, such as X-linked myopathy, adult-onset vacuolar myopathy, infantile autophagic vacuolar myopathy, and X-linked congenital autophagic vacuolar myopathy (22). Pompe disease, a severe inherited disorder of skeletal and cardiac muscle, is related to compromised autophagolysosomal degradation due to the deficiency of glycogen-degrading lysosomal enzyme acid  $\alpha$ -glucosidase (GAA) (51).

We suppose that the ability of AZT to block later stages in the autophagic process compromises the potential of myocytes to recycle and eliminate dysfunctional mitochondria generated through a previously described mechanism of NRTI-mediated mitochondrial toxicity (7, 8, 25, 26). Consequently, dysfunctional mitochondria accu-

multate and contribute to increased ROS generation and the release of proapoptotic signals (27).

Taken our findings together, our study reveals a novel mechanism of how thymidine analogues contribute to myodegenerative diseases. These data also provide evidence for an important role of autophagy in cardiac and skeletal muscle disease in HIV-infected patients.

## MATERIALS AND METHODS

**Cell culture.** The C2C12 myocyte cell line was chosen because it has been previously used as an *in vitro* model to study AZT-mediated mitochondrial myopathy (52) and was kindly provided by Martin Leverkus (Mannheim Clinic of the University of Heidelberg, Heidelberg, Germany). Cells were maintained in ATCC-formulated Eagle's minimum essential medium containing 10% fetal calf serum (FCS) with 100 U penicillin and 100  $\mu\text{g/ml}$  streptomycin and cultured as suggested in ATCC protocols.

AZT and 3TC (Sigma-Aldrich) were dissolved in dimethyl sulfoxide (DMSO) and used at concentrations that were near the therapeutic  $C_{\text{max}}$ s of AZT (6  $\mu\text{M}$ ) and 3TC (8  $\mu\text{M}$ ), as discussed elsewhere (31, 32). Higher drug concentrations (5 and 30 times the  $C_{\text{max}}$ ) were used in experiments addressing dose dependency. The following established pharmacological modulators of autophagy were used at concentrations previously reported in similar *in vitro* experiments: 3MA (5 to 10 mM), nocodazole (20 to 50  $\mu\text{M}$ ), vinblastine (20 to 50  $\mu\text{M}$ ), PP242 (1 and 5  $\mu\text{M}$ ), ammonium chloride (ACH; 10 to 20 mM), and chloroquine (5 to 10  $\mu\text{M}$ ) (28–32). 3MA, ACH, and CQ were dissolved in phosphate-buffered saline (PBS); all remaining reagents were dissolved in DMSO. Cellular viability remained unaffected even by the highest concentration (0.1% DMSO) of the solvent used in the incubation experiments.

**Constructs and retroviral infection.** pBABEpuro GFP-LC3 (plasmid 22405), generated by Jayanta Debnath (53), was purchased from Addgene. A GFP-LC3 sequence was introduced into a retroviral construct used for cell transduction. Retroviral production and cell transduction were done as previously described (54). Transduced cells were subjected to puromycin selection (1  $\mu\text{g/ml}$ ; Sigma-Aldrich, Taufkirchen, Germany) for 3 days, and GFP-positive cells were sorted by fluorescence-activated cell sorting (FACSARIA cell sorter). The development of experimental artefacts due to potential bulky GFP-LC3 aggregates was ruled out by the use of stably transduced cells and appropriate clone selection (28–32).

**Analysis of NRTI effects on cellular autophagic activity.** Autophagosomes are an intermediate component of a dynamic process, and their total quantity at a specific point of time is a function of their creation and degradation upon autophagosome-lysosome fusion (28–32). An increase in autophagosome abundance corresponds to either the induction of autophagy or the inhibition of autophagosome maturation (autophagosome-lysosome fusion). Measurement of autophagic flux allows discrimination between these two situations (28–32).

GFP-LC3 was measured by flow cytometry on the fluorescein isothiocyanate (FITC) channel or visualized by conventional fluorescence microscopy according to recently updated guidelines (28). The GFP-LC3 cytoplasmic pool was identified as a homogeneously dispersed signal, and GFP-LC3-II-labeled autophagosomes were detected as punctus formation (28).

For fluorescence microscopy, cells were washed posttreatment with 2% FCS–PBS, fixed with 4% paraformaldehyde, and analyzed on the FITC-GFP channel with an AxioImagerM1 microscope using AxioVision (version 4.8) software (Zeiss). Under each treatment condition, fluorescence images were obtained from numerous cells from several randomly chosen fields. The average number of punctae per cell was considered under each of the treated conditions. Fifty cells were randomly counted from at least 30 images per condition per experiment.

For confocal microscopy, the cells were washed posttreatment with PBS and stained with MitoTracker Deep Red, MitoTracker Green (62 nM), or MitoProbe TMRM (20 nM) diluted in trypsin-EDTA solution for 30 min in an incubator. The stained cells were then washed three times with PBS containing 2% FCS. The cells were then resuspended in PBS and centrifuged onto 1% alcian blue (catalog number A5268; Sigma-Aldrich)-treated coverslips at 2,000 rpm for 10 min, followed by fixation with 3% paraformaldehyde in PBS for 20 min. The cells were washed three times with PBS and mounted onto glass slides using mounting medium (Fluoroshield with DAPI [4',6-diamidino-2-phenylindole]; catalog number F6057; Sigma-Aldrich). The images were acquired on FITC (MTR Green), allophycocyanin (APC) (MTR Deep Red), or phycoerythrin (PE)-Texas Red (MitoProbe TMRM) using a Leica DM IRB microscope equipped with a TCS SP2 AOBs scan head (Leica, Germany) with a 63 $\times$  lens objective. Image processing was performed using LAS AF Lite (Leica, Germany), and quantification of the fluorescence intensity was achieved by using ImageJ software.

Electron microscopy (EM) was performed as previously described (32). Briefly myocytes were fixed in 150 mM HEPES, pH 7.35, containing 1.5% formaldehyde and 1.5% glutaraldehyde at room temperature for 30 min and then at 4°C overnight. After dehydration in acetone, cells were embedded in Epon resin. Sections of 50 nm were stained with 4% uranyl acetate and lead citrate and observed in a Morgagni transmission electron microscope (FEI). Images were taken with a 2K side-mounted Veleta charge-coupled-device camera. Autophagy-related structures were defined as cytoplasmic compartments enclosed by a double-limiting membrane that were not completely hollow. The limiting membranes were not decorated with ribosomes, to exclude rough endoplasmic reticulum. No remnants of cristae were visible, to exclude structures such as dead mitochondria, which also show a smooth double membrane.

Autophagic flux was also measured using a GFP-LC3 turnover assay based on flow cytometric detection of changes in the total cellular GFP-LC3 signal, as previously described (28, 32). Briefly, under conditions of increased autophagic flux, GFP-LC3 is progressively delivered to and degraded in autoly-

sosomes. Therefore, enhanced or reduced autophagic flux is detected as a decreased or an increased total cellular GFP signal, respectively (28, 32). The autophagic activity of C2C12 cells was measured essentially as previously described for Huh7, HepG2, 3T3-F442A, and K562 cells (30–32). Analysis was performed using an LSR II flow cytometer (Becton, Dickinson Biosciences), and the data for cell counts were plotted as the GFP fluorescence intensity.

**Lysosomal mass and acidity.** Lysosomal abundance and acidity were analyzed by flow cytometric measurement using LysoTracker (LTR) and LysoSensor (LSG) staining (LysoTracker Red DND-99 and LysoSensor Green DND-189, respectively; Life Technologies) according to the manufacturer's instruction and a modified protocol. Briefly, about  $5 \times 10^4$  adherent cells per well were washed once with PBS, incubated in 100  $\mu$ l of trypsin containing LTR (66 nM) or LSG (1  $\mu$ M) at 37°C in a 5% CO<sub>2</sub> incubator for 30 min, and then washed once with PBS with 2% FCS. The cells (50  $\mu$ l) were then suspended in PBS with 2% FCS, put on ice, and analyzed on a flow cytometer. Analysis was performed using an LSR II flow cytometer (Becton, Dickinson Biosciences), and the data for cell counts were plotted as the GFP fluorescence intensity for LSG or the PE-Texas Red fluorescence intensity for LTR.

**Cathepsin B and L activity.** Cathepsin B and L enzymatic activity was analyzed by flow cytometric measurement using Magic Red cathepsin L and B assay kits (ImmunoChemistry Technologies) according to the manufacturer's instructions and a modified protocol. Briefly, about  $5 \times 10^4$  adherent cells per well were washed once with PBS and incubated in 100  $\mu$ l of trypsin containing cathepsin L or B substrate (1:1,000) in a 5% CO<sub>2</sub> incubator for 30 min and then washed once with PBS–2% FCS. The cells were then suspended in 50  $\mu$ l of PBS–2% FCS, put on ice, and analyzed on a flow cytometer. Analysis was performed using an LSR II flow cytometer (Becton, Dickinson Biosciences), and the data for the cell counts were plotted as the PE-Texas Red fluorescence intensity.

**Mitochondrial mass and potential.** Intracellular mitochondrial abundance and potential were analyzed by flow cytometric analysis using MitoTracker Green (MTR Green), MitoTracker Red (MTR Red), MitoTracker Deep Red (MTR Deep Red), and MitoProbe TMRM (TMRM) stains according to the manufacturer's instructions (Molecular Probes, Eugene, OR) as previously described (32, 34). Mitochondrial potential was evaluated as the change in the ratio of potential-dependent MTR Deep Red and potential-independent MTR Green staining (34) or, alternatively as the change in mitochondrial potential-specific MitoProbe TMRM staining. Carbonyl cyanide 3-chlorophenylhydrazone (CCCP) was used as a positive control for the induction of mitochondrial membrane depolarization. Briefly, myocytes were incubated for 30 to 45 min with MTR Green, MTR Red, or MTR Deep Red (62 nM) or with TMRM (20 nM) under normal growth conditions and then analyzed using confocal microscopy or/and an LSR II flow cytometer (Becton, Dickinson Biosciences), and the data for the cell counts were plotted as the FITC, PE-Cy5, APC, and PE-Texas Red fluorescence intensity, respectively.

**Reactive oxygen species.** ROS were measured by flow cytometric analyses using 5-(and-6)-chloromethyl-2',7'-dichlorodihydrofluorescein diacetate, acetyl ester (CM-H2DCFDA), in accordance with the manufacturer's instructions (Invitrogen, Life Technologies, Darmstadt, Germany) as previously described (30, 32). Briefly, cells were incubated for 45 min with CM-H2DCFDA (2  $\mu$ M) under normal growth conditions using light protection and then put on ice and directly analyzed on the LSR II flow cytometer (Becton, Dickinson Biosciences), and the data for the cell counts were plotted as the FITC fluorescence intensity.

**Respiratory chain complexes.** The activities of respiratory chain complexes were analyzed essentially as described previously for cultured murine 3T3-L1 cells (36) and primary human adipocytes (35). C2C12 cells and their mitochondria were broken by two 10-s periods of sonication using a Sonopuls probe sonicator (Bandelin Electronic, Berlin, Germany) with single pulses of 0.3 s at 20 W of power. The activities of oxidative phosphorylation chain complexes I and III, II and III, IV (cytochrome *c* oxidase), and V (ATP synthase) were measured at 37°C as previously described comprehensively for cultured 3T3-L1 cells (36). The activity of citrate synthase, used as a mitochondrial marker enzyme, was measured. Cellular protein was measured using the method of Bensadoun and Weinstein as cited in reference 35. Positive controls for the affected respiratory chain function were run as explained earlier (35, 36).

**Cell viability.** Cell death was determined using the propidium iodide (PI) exclusion assay with flow cytometry as previously described (30, 32).

**siRNA-mediated knockdown.** C2C12 cells were transfected with ATG7-specific siRNA (catalog number 6604; Cell Signaling) for 72 h per the manufacturer's instructions, before treatment with the respective drugs. The cells were then processed as described below.

**Western blotting.** The conversion of GFP-LC3-I to GFP-LC3-II was detected by Western blotting of radioimmunoprecipitation assay buffer-extracted lysates using anti-LC3B antibody (catalog number L7543; Sigma-Aldrich) in 5% milk–2.5% bovine serum albumin as previously described (25), with  $\beta$ -actin antibody (catalog number A2103; Sigma-Aldrich) used as a loading control. The bands were visualized using secondary antibodies IRDye 800CW-conjugated goat anti-mouse IgG (H+L) (catalog number 926-32210; LI-COR, USA) and IRDye 680RD-conjugated goat anti-rabbit IgG (H+L) (catalog number 926-68071; LI-COR, USA) with the help of an Odyssey CLx infrared imaging system (LI-COR, USA). Densitometry analysis of the LC3-I and LC3-II bands was performed using Image Studio software (LI-COR, USA), and the values were expressed as the LC3-II/LC3-I ratio according to the updated recommendations (28).

**Statistics.** The evaluation of statistical significance for comparisons of more than two groups was performed by analysis of variance with Dunnett *post hoc* analysis. The level of significance was set at a *P* value of <0.05. All data are presented as the mean  $\pm$  standard deviation (SD). All calculations were performed using GraphPad Prism (version 4) software.

## SUPPLEMENTAL MATERIAL

Supplemental material for this article may be found at <https://doi.org/10.1128/AAC.01443-18>.

**SUPPLEMENTAL FILE 1**, PDF file, 0.2 MB.

## ACKNOWLEDGMENTS

G.M.N.B. was supported by the German Research Foundation (KFO 250, TP1) and the Excellence Cluster From Regenerative Biology to Reconstructive Therapy (EXC 62/1). D.P.-D. was supported by the German Research Foundation (Le 953/8-1).

We thank the N. Mizushima and B. Levine laboratories for valuable methodological advice, Marion Hitzgrath and Roland Jacobs for technical assistance, and Thomas Lücke and Anibh Das for help with measurement of respiratory chain activity. We acknowledge the technical assistance of the members of the MHH Core Facility for Cell Sorting.

This research received no specific grant from any funding agency in the public, commercial, or not-for-profit sector.

We report no conflict of interest.

## REFERENCES

- Lewis W, Dalakas MC. 1995. Mitochondrial toxicity of antiviral drugs. *Nat Med* 1:417–422. <https://doi.org/10.1038/nm0595-417>.
- Lewis W, Gonzalez B, Chomyn A, Papoian T. 1992. Zidovudine induces molecular, biochemical, and ultrastructural changes in rat skeletal muscle mitochondria. *J Clin Invest* 89:1354–1360. <https://doi.org/10.1172/JCI115722>.
- Lewis W, Grupp IL, Grupp G, Hoit B, Morris R, Samarel AM, Bruggeman L, Klotman P. 2000. Cardiac dysfunction occurs in the HIV-1 transgenic mouse treated with zidovudine. *Lab Invest* 80:187–197. <https://doi.org/10.1038/labinvest.3780022>.
- Bolhaar MG, Karstaedt AS. 2007. A high incidence of lactic acidosis and symptomatic hyperlactatemia in women receiving highly active antiretroviral therapy in Soweto, South Africa. *Clin Infect Dis* 45:254–260. <https://doi.org/10.1086/518976>.
- Osler M, Stead D, Rebe K, Meintjes G, Boule A. 2010. Risk factors for and clinical characteristics of severe hyperlactataemia in patients receiving antiretroviral therapy: a case-control study. *HIV Med* 11:121–129. <https://doi.org/10.1111/j.1468-1293.2009.00754.x>.
- Zhang P, Zhang L, Jiang Z, Xiong Y, Chen H, Tao Y, Hu M, Li Z. 2011. Evaluation of mitochondrial toxicity in Marmota himalayana treated with metacavir, a novel 2',3'-dideoxyguanosine prodrug for treatment of hepatitis B virus. *Antimicrob Agents Chemother* 55:1930–1936. <https://doi.org/10.1128/AAC.01520-10>.
- Brinkman K, ter Hofstede HJ, Burger DM, Smeitink JA, Koopmans PP. 1998. Adverse effects of reverse transcriptase inhibitors: mitochondrial toxicity as common pathway. *AIDS* 12:1735–1744. <https://doi.org/10.1097/00002030-199814000-00004>.
- Walker UA, Setzer B, Venhoff N. 2002. Increased long-term mitochondrial toxicity in combinations of nucleoside analogue reverse-transcriptase inhibitors. *AIDS* 16:2165–2173. <https://doi.org/10.1097/00002030-200211080-00009>.
- Payne BA, Wilson IJ, Hateley CA, Horvath R, Santibanez-Koref M, Samuels DC, Price DA, Chinnery PF. 2011. Mitochondrial aging is accelerated by anti-retroviral therapy through the clonal expansion of mtDNA mutations. *Nat Genet* 43:806–810. <https://doi.org/10.1038/ng.863>.
- Kohler JJ, Cucoranu I, Fields E, Green E, He S, Hoying A, Russ R, Abuin A, Johnson D, Hosseini SH, Raper CM, Lewis W. 2009. Transgenic mitochondrial superoxide dismutase and mitochondrially targeted catalase prevent antiretroviral-induced oxidative stress and cardiomyopathy. *Lab Invest* 89:782–790. <https://doi.org/10.1038/labinvest.2009.39>.
- Kohler JJ, Hosseini SH, Cucoranu I, Hoying-Brandt A, Green E, Johnson D, Wittich B, Srivastava J, Ivey K, Fields E, Russ R, Raper CM, Santoianni R, Lewis W. 2009. Murine cardiac mtDNA: effects of transgenic manipulation of nucleoside phosphorylation. *Lab Invest* 89:122–130. <https://doi.org/10.1038/labinvest.2008.121>.
- Velsor LW, Kovacevic M, Goldstein M, Leitner HM, Lewis W, Day BJ. 2004. Mitochondrial oxidative stress in human hepatoma cells exposed to stavudine. *Toxicol Appl Pharmacol* 199:10–19. <https://doi.org/10.1016/j.taap.2004.03.005>.
- Apostolova N, Blas-García A, Esplugues JV. 2011. Mitochondrial toxicity in HAART: an overview of in vitro evidence. *Curr Pharm Des* 17:2130–2144. <https://doi.org/10.2174/138161211796904731>.
- Brinkman K, Smeitink JA, Romijn JA, Reiss P. 1999. Mitochondrial toxicity induced by nucleoside-analogue reverse-transcriptase inhibitors is a key factor in the pathogenesis of antiretroviral-therapy-related lipodystrophy. *Lancet* 354:1112–1115. [https://doi.org/10.1016/S0140-6736\(99\)06102-4](https://doi.org/10.1016/S0140-6736(99)06102-4).
- McKenzie R, Fried MW, Sallie R, Conjeevaram H, Di Bisceglie AM, Park Y, Savarese B, Kleiner D, Tsokos M, Luciano C, Pruetz T, Stotka JL, Straus SE, Hoofnagle JH. 1995. Hepatic failure and lactic acidosis due to fialuridine (FIAU), an investigational nucleoside analogue for chronic hepatitis B. *N Engl J Med* 333:1099–1105. <https://doi.org/10.1056/NEJM199510263331702>.
- Dalakas MC, Illa I, Pezeshkpour GH, Laukaitis JP, Cohen B, Griffin JL. 1990. Mitochondrial myopathy caused by long-term zidovudine therapy. *N Engl J Med* 322:1098–1105. <https://doi.org/10.1056/NEJM199004193221602>.
- Nomura R, Sato T, Sato Y, Medin JA, Kushimoto S, Yanagisawa T. 2017. Azidothymidine-triphosphate impairs mitochondrial dynamics by disrupting the quality control system. *Redox Biol* 13:407–417. <https://doi.org/10.1016/j.redox.2017.06.011>.
- Koczor CA, Jiao Z, Fields E, Russ R, Ludaway T, Lewis W. 2015. AZT-induced mitochondrial toxicity: an epigenetic paradigm for dysregulation of gene expression through mitochondrial oxidative stress. *Physiol Genomics* 47:447–454. <https://doi.org/10.1152/physiolgenomics.00045.2015>.
- Boya P, Gonzalez-Polo RA, Casares N, Perfettini JL, Dessen P, Larochette N, Metivier D, Meley D, Souquere S, Yoshimori T, Pierron G, Codogno P, Kroemer G. 2005. Inhibition of macroautophagy triggers apoptosis. *Mol Cell Biol* 25:1025–1040. <https://doi.org/10.1128/MCB.25.3.1025-1040.2005>.
- Kanki T, Klionsky DJ. 2010. The molecular mechanism of mitochondria autophagy in yeast. *Mol Microbiol* 75:795–800. <https://doi.org/10.1111/j.1365-2958.2009.07035.x>.
- Zhang Y, Qi H, Taylor R, Xu W, Liu LF, Jin S. 2007. The role of autophagy in mitochondria maintenance: characterization of mitochondrial functions in autophagy-deficient *S. cerevisiae* strains. *Autophagy* 3:337–346. <https://doi.org/10.4161/auto.4127>.
- Levine B, Kroemer G. 2008. Autophagy in the pathogenesis of disease. *Cell* 132:27–42. <https://doi.org/10.1016/j.cell.2007.12.018>.
- Nishino I, Fu J, Tanji K, Yamada T, Shimojo S, Koori T, Mora M, Riggs JE, Oh SJ, Koga Y, Sue CM, Yamamoto A, Murakami N, Shanske S, Byrne E, Bonilla E, Nonaka I, DiMauro S, Hirano M. 2000. Primary LAMP-2 deficiency causes X-linked vacuolar cardiomyopathy and myopathy (Danon disease). *Nature* 406:906–910. <https://doi.org/10.1038/35022604>.
- Nakai A, Yamaguchi O, Takeda T, Higuchi Y, Hikoso S, Taniike M, Omiya S, Mizote I, Matsumura Y, Asahi M, Nishida K, Hori M, Mizushima N, Otsu K. 2007. The role of autophagy in cardiomyocytes in the basal state and in response to hemodynamic stress. *Nat Med* 13:619–624. <https://doi.org/10.1038/nm1574>.



25. Cote HC. 2005. Possible ways nucleoside analogues can affect mitochondrial DNA content and gene expression during HIV therapy. *Antivir Ther* 10(Suppl 2):M3–M11.
26. Lewis W. 2005. Nucleoside reverse transcriptase inhibitors, mitochondrial DNA and AIDS therapy. *Antivir Ther* 10(Suppl 2):M13–M27.
27. Colell A, Ricci JE, Tait S, Milasta S, Maurer U, Bouchier-Hayes L, Fitzgerald P, Guio-Carrion A, Waterhouse NJ, Li CW, Mari B, Barbry P, Newmeyer DD, Beere HM, Green DR. 2007. GAPDH and autophagy preserve survival after apoptotic cytochrome c release in the absence of caspase activation. *Cell* 129:983–997. <https://doi.org/10.1016/j.cell.2007.03.045>.
28. Klionsky DJ, Abdelmohsen K, Abe A, Abedin MJ, Beliovich H, Acevedo Arozena A, Adachi H, Adams CM, Adams PD, Adeli K, Adhietty PJ, Adler SG, Agam G, Agarwal R, Aghi MK, Agnello M, Agostinis P, Aguilar PV, Aguirre-Ghiso J, Airolidi EM, Ait-Si-Ali S, Akematsu T, Akporiaye ET, Al-Rubeai M, Albaiceta GM, Albanese C, Albani D, Albert ML, Aldudo J, Algül H, Alirezai M, Alloza I, Almasan A, Almonte-Beceril M, Alnemri ES, Alonso C, Altan-Bonnet N, Altieri DC, Alvarez S, Alvarez-Erviti L, Alves S, Amadoro G, Amano A, Amantini C, Ambrosio S, Amelio I, Amer AO, Amessou M, Amon A, An Z, et al. 2016. Guidelines for the use and interpretation of assays for monitoring autophagy (3rd edition). *Autophagy* 12:1–222. <https://doi.org/10.1080/15548627.2015.1100356>.
29. Klose J, Stankov MV, Kleine M, Ramackers W, Panayotova-Dimitrova D, Jager MD, Klemptner J, Winkler M, Bektas H, Behrens GM, Vondran FW. 2014. Inhibition of autophagic flux by salinomycin results in anti-cancer effect in hepatocellular carcinoma cells. *PLoS One* 9:e95970. <https://doi.org/10.1371/journal.pone.0095970>.
30. Stankov MV, El Khatib M, Kumar Thakur B, Heitmann K, Panayotova-Dimitrova D, Schoening J, Bourquin JP, Schweitzer N, Leverkus M, Welte K, Reinhardt D, Li Z, Orkin SH, Behrens GM, Klusmann JH. 2014. Histone deacetylase inhibitors induce apoptosis in myeloid leukemia by suppressing autophagy. *Leukemia* 28:577–588. <https://doi.org/10.1038/leu.2013.264>.
31. Stankov MV, Panayotova-Dimitrova D, Leverkus M, Schmidt RE, Behrens GM. 2013. Thymidine analogues suppress autophagy and adipogenesis in cultured adipocytes. *Antimicrob Agents Chemother* 57:543–551. <https://doi.org/10.1128/AAC.01560-12>.
32. Stankov MV, Panayotova-Dimitrova D, Leverkus M, Vondran FW, Bauerfeind R, Binz A, Behrens GM. 2012. Autophagy inhibition due to thymidine analogues as novel mechanism leading to hepatocyte dysfunction and lipid accumulation. *AIDS* 26:1995–2006. <https://doi.org/10.1097/QAD.0b013e32835804f9>.
33. Gottlieb RA, Carreira RS. 2010. Autophagy in health and disease. 5. Mitophagy as a way of life. *Am J Physiol Cell Physiol* 299:C203–C210. <https://doi.org/10.1152/ajpcell.00097.2010>.
34. Zhou R, Yazdi AS, Menu P, Tschopp J. 2011. A role for mitochondria in NLRP3 inflammasome activation. *Nature* 469:221–225. <https://doi.org/10.1038/nature09663>.
35. Stankov MV, Lucke T, Das AM, Schmidt RE, Behrens GM. 2010. Mitochondrial DNA depletion and respiratory chain activity in primary human subcutaneous adipocytes treated with nucleoside analogue reverse transcriptase inhibitors. *Antimicrob Agents Chemother* 54:280–287. <https://doi.org/10.1128/AAC.00914-09>.
36. Stankov MV, Lucke T, Das AM, Schmidt RE, Behrens GM, German Competence Network HIV/AIDS. 2007. Relationship of mitochondrial DNA depletion and respiratory chain activity in preadipocytes treated with nucleoside reverse transcriptase inhibitors. *Antivir Ther* 12:205–216.
37. Settembre C, Ballabio A. 2011. TFEB regulates autophagy: an integrated coordination of cellular degradation and recycling processes. *Autophagy* 7:1379–1381. <https://doi.org/10.4161/auto.7.11.17166>.
38. Settembre C, Di Malta C, Polito VA, Garcia Arencibia M, Vetrini F, Erdin S, Erdin SU, Huynh T, Medina D, Colella P, Sardiello M, Rubinsztein DC, Ballabio A. 2011. TFEB links autophagy to lysosomal biogenesis. *Science* 332:1429–1433. <https://doi.org/10.1126/science.1204592>.
39. Cuervo AM. 2011. Cell biology. Autophagy's top chef. *Science* 332:1392–1393. <https://doi.org/10.1126/science.1208607>.
40. Roczniak-Ferguson A, Petit CS, Froehlich F, Qian S, Ky J, Angarola B, Walther TC, Ferguson SM. 2012. The transcription factor TFEB links mTORC1 signaling to transcriptional control of lysosomal homeostasis. *Sci Signal* 5:ra42. <https://doi.org/10.1126/scisignal.2002790>.
41. Aits S, Jaattela M. 2013. Lysosomal cell death at a glance. *J Cell Sci* 126:1905–1912. <https://doi.org/10.1242/jcs.091181>.
42. Dai DF, Johnson SC, Villarín JJ, Chin MT, Nieves-Cintrón M, Chen T, Marcinek DJ, Dorn GW, II, Kang YJ, Prolla TA, Santana LF, Rabinovitch PS. 2011. Mitochondrial oxidative stress mediates angiotensin II-induced cardiac hypertrophy and Galphaq overexpression-induced heart failure. *Circ Res* 108:837–846. <https://doi.org/10.1161/CIRCRESAHA.110.232306>.
43. Dai DF, Rabinovitch P. 2011. Mitochondrial oxidative stress mediates induction of autophagy and hypertrophy in angiotensin-II treated mouse hearts. *Autophagy* 7:917–918. <https://doi.org/10.4161/auto.7.8.15813>.
44. Dai DF, Santana LF, Vermulst M, Tomazela DM, Emond MJ, MacCoss MJ, Gollahon K, Martin GM, Loeb LA, Ladiges WC, Rabinovitch PS. 2009. Overexpression of catalase targeted to mitochondria attenuates murine cardiac aging. *Circulation* 119:2789–2797. <https://doi.org/10.1161/CIRCULATIONAHA.108.822403>.
45. Neubauer S. 2003. Cardiac magnetic resonance spectroscopy. *Curr Cardiol Rep* 5:75–82. <https://doi.org/10.1007/s11886-003-0041-0>.
46. Neubauer S. 2007. The failing heart—an engine out of fuel. *N Engl J Med* 356:1140–1151. <https://doi.org/10.1056/NEJMra063052>.
47. Elmore SP, Qian T, Grissom SF, Lemasters JJ. 2001. The mitochondrial permeability transition initiates autophagy in rat hepatocytes. *FASEB J* 15:2286–2287. <https://doi.org/10.1096/fj.01-0206fj>.
48. Terman A, Brunk UT. 2005. Autophagy in cardiac myocyte homeostasis, aging, and pathology. *Cardiovasc Res* 68:355–365. <https://doi.org/10.1016/j.cardiores.2005.08.014>.
49. Tanaka Y, Guhde G, Suter A, Eskelinen EL, Hartmann D, Lullmann-Rauch R, Janssen PM, Blanz J, von Figura K, Saftig P. 2000. Accumulation of autophagic vacuoles and cardiomyopathy in LAMP-2-deficient mice. *Nature* 406:902–906. <https://doi.org/10.1038/35022595>.
50. Bolanos-Meade J, Zhou L, Hoke A, Corse A, Vogelsang G, Wagner KR. 2005. Hydroxychloroquine causes severe vacuolar myopathy in a patient with chronic graft-versus-host disease. *Am J Hematol* 78:306–309. <https://doi.org/10.1002/ajh.20294>.
51. Fukuda T, Ahearn M, Roberts A, Mattaliano RJ, Zaal K, Ralston E, Plotz PH, Raben N. 2006. Autophagy and mistargeting of therapeutic enzyme in skeletal muscle in Pompe disease. *Mol Ther* 14:831–839. <https://doi.org/10.1016/j.yymthe.2006.08.009>.
52. d'Amati G, Lewis W. 1994. Zidovudine causes early increases in mitochondrial ribonucleic acid abundance and induces ultrastructural changes in cultured mouse muscle cells. *Lab Invest* 71:879–884.
53. Fung C, Lock R, Gao S, Salas E, Debnath J. 2008. Induction of autophagy during extracellular matrix detachment promotes cell survival. *Mol Biol Cell* 19:797–806. <https://doi.org/10.1091/mbc.e07-10-1092>.
54. Diessenbacher P, Hupe M, Sprick MR, Kerstan A, Geserick P, Haas TL, Wachter T, Neumann M, Walczak H, Silke J, Leverkus M. 2008. NF-kappaB inhibition reveals differential mechanisms of TNF versus TRAIL-induced apoptosis upstream or at the level of caspase-8 activation independent of cIAP2. *J Invest Dermatol* 128:1134–1147. <https://doi.org/10.1038/sj.jid.5701141>.